Acta Materialia 215 (2021) 117014

Contents lists available at ScienceDirect

Acta Materialia

journal homepage: www.elsevier.com/locate/actamat

Full length article

Natural and artificial ageing in aluminium alloys – the role of excess vacancies

Zi Yang, John Banhart*

Helmholtz-Centre Berlin for Materials and Energy, Hahn-Meitner-Platz 1, 14109 Berlin, Germany

ARTICLE INFO

Article history:
Received 21 February 2021
Revised 13 April 2021
Accepted 20 May 2021
Available online 26 May 2021

Keywords:
Aluminium Alloy
Vacancy
Diffusion
Age hardening
Kinetics
Al-Mg-Si

ABSTRACT

Non-equilibrium excess vacancies quenched-in after solutionising age-hardenable aluminium alloys at high temperature are known to play an important role in precipitation at lower temperatures. However, knowledge is still lacking on the extent of the contribution to precipitation at various temperatures. In this work, we revisit this classical problem and study the role of excess vacancies in an Al-Mg-Si alloy in natural and artificial ageing experimentally by hardness measurements, differential scanning calorimetry, and positron annihilation lifetime spectroscopy. We then apply a precipitation model involving a simulation of vacancy loss and solute diffusion based on parameters calculated by first principles. The experiments show that excess vacancies are largely removed in the initial seconds of artificial ageing with hardly any corresponding hardening, i.e., subsequent hardening is triggered primarily by equilibrium vacancies unlike natural ageing, where hardening is mainly driven by excess vacancies. We reproduce the anomaly that hardening for a given time can be faster at lower temperatures and explain this by the different activation energies of vacancy annihilation and solute diffusion. The role of excess vacancies demonstrated in Al-Mg-Si alloys could be similar in other age-hardenable alloys and hence be a universal phenomenon.

1. Introduction

Precipitation strengthening in aluminium alloys involves dissolving solute atoms in the aluminium lattice at high temperatures, preserving the resulting solid solution by quenching, and ageing the alloy, during which solute atoms diffuse through the matrix and form clusters (small disordered solute agglomerations on the fcc lattice), zones or precipitates (ordered solute complexes with an own lattice structure, but terminologies vary) and increase strength (or hardness). Two common terms are in use to describe age hardening: 'natural ageing' (NA) and 'artificial ageing' (AA): The former is carried out at 'room temperature', the latter at 'elevated temperatures' [1]. 'Room temperature' is usually not defined and could range from 'quite cold' in a laboratory in Norway to 'rather hot' in a production plant in Qatar. In view of the known strong temperature sensitivity of ageing processes [2] the term NA appears inadequate. 'Artificial ageing' is carried out between 150 °C and 190 °C for most commercial aluminium alloys. But what is the physical difference between natural and artificial ageing, where is the transition between the two and what is special about 'room temperature'?

AA leads to a different range of precipitate types than NA and usually higher hardness or strength levels are reached. For Al-Mg-Si alloys, it has been claimed that there is a transition temperature above which the kind of the precipitates formed during ageing differs from that below and the transition temperature is seen at around 67 °C [3]. Differences noted include that NA clusters formed at low temperatures can differ in composition from AA clusters [4-6] (however with sometimes controversial results from such atom probe studies), contain more vacancies [7-9] or differ in structure and size. NA clusters might not [10] or only partially [6] be able to grow during subsequent AA. However, such distinctions rather describe the result of different processes than their origin.

It has been known for a long time that ageing at 'room temperature' is many orders of magnitude faster than estimated from extrapolated equilibrium diffusion coefficients of solute atoms. An answer for this finding was given by authors in the 1950s: excess vacancies frozen-in during quenching accelerate the precipitation rate during NA sufficiently to explain the observed hardening rates [11,12]. The distinct stages during NA often involve a fast and a slow reaction that can be explained by excess vacancies that increasingly anneal out or are trapped by clusters [13]. Surprisingly, NA can be faster than AA although it takes place at much lower temperature: Hardness [14], thermoelectric power [15] or electrical

* Corresponding author.
E-mail address: banhart@helmholtz-berlin.de (J. Banhart).

https://doi.org/10.1016/j.actamat.2021.117014
1359-6454/

resistivity [16,17] can change at a higher rate at a lower temperature in certain stages of ageing. At first sight, this appears counter-intuitive and requires an explanation.

Positron lifetime experiments indeed show the presence of excess vacancies directly after quenching in Al-Mg-Si alloys [2]. However, the exact role of excess vacancies in ageing processes at various temperatures has not yet been clearly discussed or modelled. The transition between natural and artificial ageing regimes is not clear. For how long and up to which ageing temperature do excess vacancies play a dominant role?

In this report, we experimentally investigate the role of vacancies in ageing processes at various temperatures and support the conclusions by simulations. The main point to show is that natural ageing can be primarily defined as a process that is determined by temporarily available excess vacancies in the alloy during quenching and ageing, whereas artificial ageing is governed mostly by permanently available equilibrium vacancies. Some of the facts discussed have been noted before, but not in a general frame and in a quantitative way.

2. Experimental

2.1. Material and heat treatment

An alloy 6014 was used in this study since it is well characterised and due to its small grain size hardness measurements scatter little. The alloy was supplied by Novelis R&D Centre Sierre and is the same used in two previous studies [18,19]. It contains 0.65% Mg, 0.60% Si, 0.18% Fe, 0.08% Mn, 0.12% Cu, all in wt.%, as the main alloying elements of aluminium. Solutionising was done at 540 °C for 1 h in an air circulation furnace, after which the samples were dropped into ice water or slowly cooled in air to 200 °C at 5 $K \cdot s^{-1}$ (average from 533 °C to 250 °C) and then quenched in ice water ('AC_200') [19]. Ageing was carried out in various devices: A Peltier-cooled incubator was used for ageing from 5 °C to 20 °C (±0.1 K), a liquid metal bath for short ageing at 160 °C or 180 °C (±1 K) to ensure the high heating rate needed for treatments that last only seconds (for example, it takes 0.9 s to reach 170 °C if the bath is at 180 °C [20]). Longer ageing treatments from 35 °C to 180 °C were done in an oil bath (±0.2 K).

2.2. Methods

Brinell hardness was measured using a Qness60M tester and a load of 10 kg-force applied with a tungsten carbide indenter of 1 mm diameter. Eight indentations were performed on each sample and averaged. The corresponding standard deviation was <1 HBW for >98% of the measurements.

Differential scanning calorimetry (DSC) measurements were carried out in a Netzsch DSC 204F1 Phoenix unit from 10 °C to 400 °C at a heating rate of 10 $K \cdot min^{-1}$. Disks of 4.8 mm diameter were punched out of both the actual alloy and the pure aluminium used as a reference. The double ramp method described earlier was applied for the baseline correction since it ensures a small baseline drift [18].

Positron lifetime measurements are based on the following principle: Positrons emerge from a radioactive ^{22}Na source – activity 0.5 MBq – encapsulated in a Kapton foil and sandwiched between two identical alloy samples, dimensions (10 × 10 × 1) mm^3. These positrons annihilate in the alloy and generate characteristic 511 keV radiation which is detected. A timing system determines the lifetime of a specific positron by correlating this event with the start signal emitted when the positron is generated in the decay process. Typically 10^5 events are summed up to a spectrum, which is background and source corrected and a positron lifetime determined. Such a low number of counts was found to be sufficient to determine the time-dependent one-component positron lifetime τ_{1C} during NA [2]. Positron lifetime measurements were carried out directly after quenching or after short artificial ageing, and further ~3 min of sample handling at 20 ± 2 °C. As during measurement at 20 ± 2 °C, the positron lifetime evolves, it is measured continuously for at least 1 h and back-extrapolated to the time of quench as demonstrated in the supplement of Ref. [20]. More details of the measurement and equipment have been published elsewhere [21].

3. Experiments and preliminary discussion

3.1. Hardness

Fig. 1a shows how the hardness of alloy 6014 evolves during isothermal treatment at different temperatures. A common feature is the increase in hardness as ageing proceeds. Overageing is seen above 160 °C and might eventually also occur for lower temperatures and longer times. Notably, there is a range, where ageing at lower temperature leads to higher hardness than ageing at higher temperature for the same time, namely for a few hours.

This crossover is more evident if one displays hardness as a function of temperature for various selected ageing times, see Fig. 1b. For any ageing time, a first maximum of hardness is observed between 20 °C and 65 °C, after which hardness decreases before increasing again to another maximum value at 140 °C or higher. At the highest temperatures, softening has set in. Stages I and III show 'normal' behaviour: If for a given ageing time the temperature is higher, a higher degree of precipitation is expected due to thermal activation of the diffusion processes that cause precipitation. Stage IV occurs because ageing at very high temperatures leads to coarser precipitates, which are less effective in hardening, also known as over-ageing. The anomaly is stage II: Here, an increase of temperature leads to a lower hardness in a given time. For example, ageing for 4 h at 35 °C leads to a higher strength than 4 h at 65 °C (magenta coloured line in Fig. 1b). This hardening anomaly in Fig. 1b is a fundamental effect also observed in other alloys as can be seen by re-drawing data for Al-Cu-Mg [22] and Al-Zn-Mg [23] alloys in that way. For another Al-Mg-Si alloy, Ref. [14] provides similar data and analysis, however, without giving microscopic explanations for the various stages.

The idea developed in this paper is that stage II (and the double-peak structure in Fig. 1b) can be explained by the contribution of excess vacancies to precipitation at various temperatures without referring to more complex concepts such as nucleation theories or models of strengthening by clusters and precipitates. More specifically, excess vacancies play a predominant role at low temperatures and overcompensate the lower thermal activation of solute migration. This effect weakens as temperature increases and eventually fades for AA at high temperatures. In a first step, we collect evidence that AA is indeed governed predominantly by equilibrium vacancies.

3.2. DSC

DSC measures thermal effects caused by precipitation during linear heating. A well-studied example is an alloy in the as-quenched state. Data for the current alloy is shown in Fig. 2a (black curve). The various peaks in the trace can be ascribed to the formation of clusters (at ~80 °C), β" phase (at ~250 °C), and β' phase (at ~300 °C) [24,25]. Pre-treatment before DSC varies the conditions for precipitation and leads to changes of the trace. Fig. 2 demonstrates that the DSC trace is changed differently by pre-ageing at AA temperatures (a, b) or at 20 °C (c). We focus

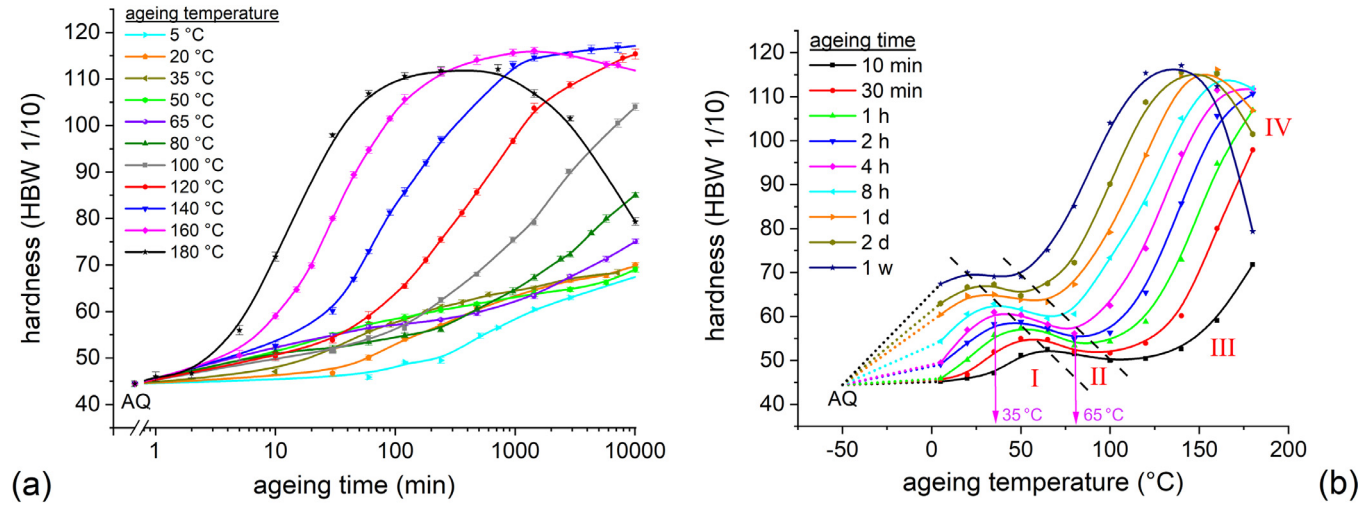

Fig. 1. Isothermal hardening curves after solutionising and quenching of alloy 6014. a) Given as a function of time for 11 different ageing temperatures, b) Displayed as a function of temperature for 9 different ageing times (some data obtained by interpolation/extrapolation of a). The dotted lines denote the known freezing out of ageing for 1 week at −50 °C [52], which was not measured here. 4 different stages are separated by dashed lines and numbered I to IV.

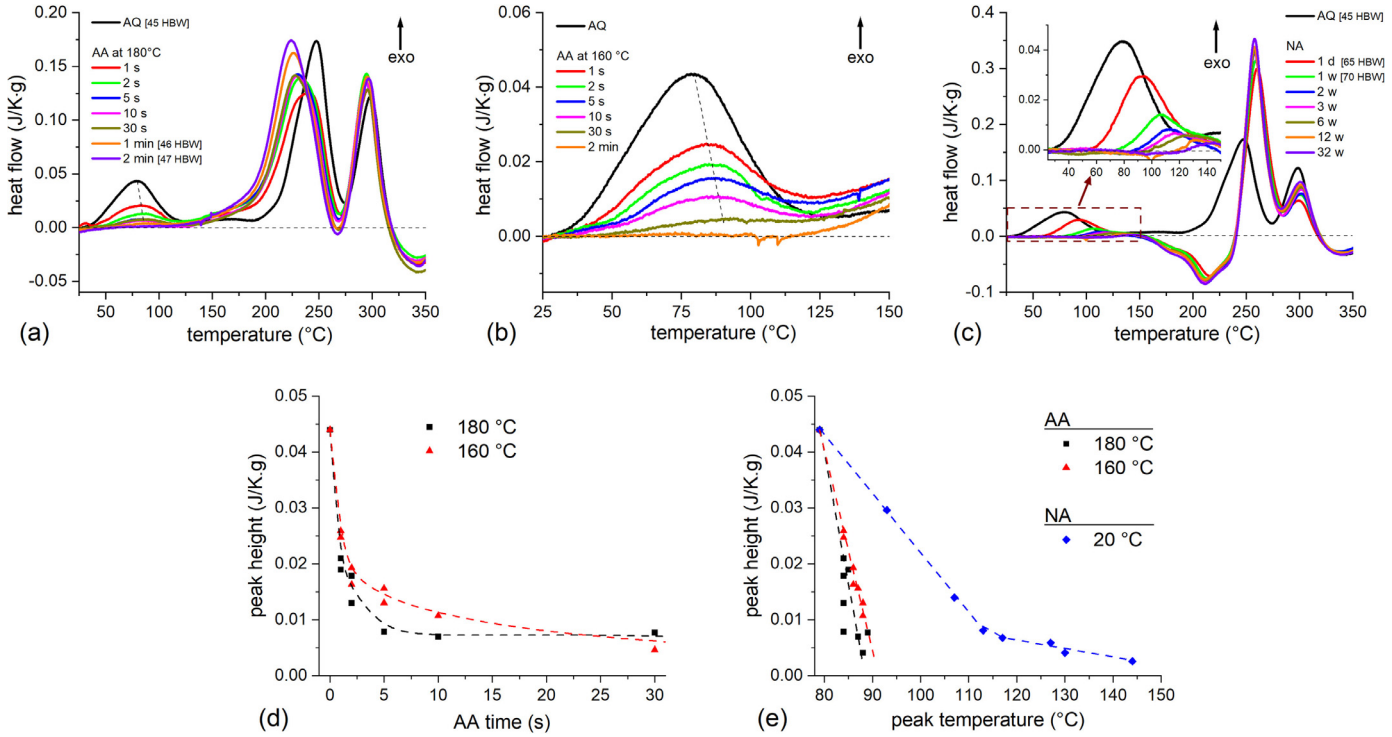

Fig. 2. (a–c) DSC traces measured on alloy 6014 at 10 K·min^{-1} directly after quenching ('AQ') and after various pre-ageing treatments at: a) 180 °C for 1 s up to 2 min, b) 160 °C for 1 s up to 2 min with only the first peak shown, and c) 20 °C for up to 32 weeks. Inset in (c) also shows the first peak magnified. Hardness values for some ageing conditions are given in the legends of a) and c). (d, e) Analyses of the first peak in the DSC traces in (a–c): d) Height of the peaks in (a, b) shown as a function of ageing time (including some repeated measurements). e) Height of the peak shown as a function of peak temperature for (a–c).

here on the first peak since it is closely related to the state after pre-ageing. Fig. 2a shows that the cluster peak is largely reduced even by the shortest treatment (1 s, including 0.9 s heating time) applied at 180 °C. With 5 s to 10 s of AA applied, the peak is largely eliminated and it is completely suppressed after 2 min of pre-ageing. A similar behaviour is observed when AA is at 160 °C (Fig. 2b), only that the peak reduction is slower than at 180 °C as summarised in Fig. 2d. Hardening of the alloy during such short ageing is very little, with only <3 HBW observed for ageing at 180 °C for 2 min (see legend of Fig. 2a). This is very different from what we see when NA before DSC is applied (Fig. 2c). There, longer ageing also reduces the amplitude of the cluster peak, but pronounced hardening occurs long before the peak is notably reduced. Another noteworthy feature is the position of the peak: it is only slightly influenced by ageing at 180 °C before DSC measurement (+10 K) but is shifted much more (+65 K) by prior ageing at 20 °C (Fig. 2e).

The reason for the occurrence of a cluster peak in Fig. 2a points at fast precipitation up to 125 °C in a short time (~10 min at the heating rate chosen). The pre-requisites for this are a high solute supersaturation and a high excess vacancy fraction. Short ageing at 160 °C or 180 °C removes the clustering peak without causing

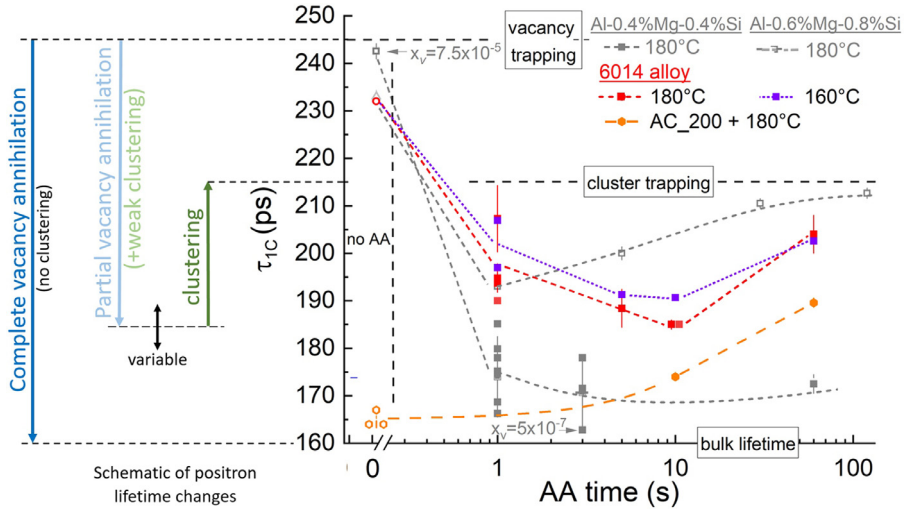

Fig. 3. One-component positron lifetimes τ_{1C} after various heat treatments: Open symbols in area 'no AA': samples quenched into ice water, except for the orange symbol where samples were slowly air cooled to 200 °C at an average rate of 5 K·s^{-1} and then quenched in ice water ('AC_200'). Solid symbols: Artificially aged samples. Alloys are ternary model alloys Al-0.4%Mg-0.4%Si and Al-0.6%Mg-0.8%Si [20] and current alloy 6014. Vacancy site fractions in grey are from Ref. [20]. Various typical positron lifetimes are marked by boxes. The arrows on the left visualise the changes of positron lifetime τ_{1C} when vacancies are lost and clustering occurs in parallel or after.

measurable hardening (even up to 2 min, see legend of Fig. 2a), i.e. it is the rapid loss of excess vacancies and not of solutes during short AA that reduces clustering so much that it no longer can be detected by DSC.

In contrast, during slow removal of excess vacancies during NA, clusters are formed and cause significant hardening (see legend of Fig. 2c). We suggest that the clusters formed during NA act back on vacancies by trapping them. Thus, the cluster peak in the low-temperature regime of the ensuing DSC run is markedly reduced. As binding weakens at increasing temperatures, vacancies are released back into the matrix and assist further clustering. As a result, the annihilation of excess vacancies during DSC scanning is buffered by NA clusters, which causes the shift of the cluster peak to higher temperatures. In Section 4, we further validate these arguments by simulations.

3.3. Positron lifetime

To further support the statement that vacancies are removed quickly during artificial ageing we carry out positron lifetime measurements. In the Al-Mg-Si alloys treated here, annihilation of positrons in three different ways is considered [21], each one being represented by a typical lifetime value: (i) annihilation in the aluminium matrix outside defects gives rise to a lifetime component $\tau_1 \leq 160$ps, (ii) annihilation in clusters and coherent precipitates (e.g. β") contributes to a positron lifetime component $\tau_2 \cong 215$ps and, (iii) positrons trapped in vacancies (free or attached to solutes or small clusters) contribute $\tau_3 \cong 245$ps. Ignoring variations of each of these contributions caused by chemical and structural variations of the positron trap is a first approximation [20]. Equating the weighted average of these contributions, $\bar{\tau}$, to the measured τ_{1C} is a second, which we have shown to be valid except for few special cases (see supplement of Ref. [20]). The τ_{1C} we measure is therefore an average of three annihilation pathways.

In the 'AQ' state after ice water quenching, a high positron lifetime $\geq$230 ps is obtained in alloy 6014, see Fig. 3. It is caused by the annihilation of a large fraction of positrons in vacancies or vacancy-solute complexes. When ageing at 180 °C for just a few seconds, a pronounced decrease of positron lifetime by ~40 ps down to ~190 ps is measured, indicating that the vacancy fraction has dropped markedly, so that many positrons now annihilate in the Al bulk where the lifetime is just 160 ps. In a lean alloy Al-0.4%Mg-0.4%Si, τ_{1C} drops even more to just 163 ps within seconds of ageing, which is even closer to defect-free aluminium [20], see blue arrow on the very left of Fig. 3. The corresponding vacancy site fractions given in Fig. 3 were derived using the trapping model for positrons [20]. The decrease of positron lifetime caused by short ageing terminates at a higher value in the more concentrated alloy 6014 than in the lean alloy Al-0.4%Mg-0.4%Si (with variations among other alloys such as Al-0.6%Mg-0.8%Si and different ageing temperatures, see double sided arrow in Fig. 3). This is because solute clusters and precipitates are formed during and after quenching [21], which strongly trap positrons in competition to bulk and vacancy-related defects and mix into the measured τ_{1C} with a typical lifetime of ~215 ps. We normally cannot distinguish between the various contributions and just notice a limited decrease, after which continuing clustering eventually brings τ_{1C} up towards ~215 ps (dark green arrow).

This interpretation is supported by the measurement of the 'AC_200' samples that due to their quenching history contain very few excess vacancies after quenching [19] and in which the positron lifetime is very low at ~165 ps. Subsequent short ageing at 180 °C for up to 1 min increases positron lifetime by ~20 ps, suggesting that it is sensitive even to the small amount of clusters formed (green arrow in Fig. 3). For this reason, we cannot specify the extent of vacancy loss during short ageing quantitatively in such alloys, but obtain a confirmation of the fast loss kinetics.

We have shown that AA takes place after most excess vacancies have been removed. Next, we would like to prove that NA is enabled by excess vacancies. Positron lifetime measurements do not allow us to follow the vacancy site fraction in alloy samples during NA quantitatively due to positron trapping dominated by clusters. Therefore, we will model the precipitation behaviour in our alloy based on a model for vacancy annihilation and precipitate growth and show that it exactly predicts this role of excess vacancies.

4. Simulations

We strengthen our arguments by simulating the clustering/precipitation process. Our aim is not to exactly represent the kinetics of the ageing processes, which is difficult due to its complex nature, but to semi-quantitatively explain the experimental observations in the context of precipitation under non-equilibrium vacancy kinetics using simple, yet physics-based models. We first

describe the model (Section 4.1), which accounts for precipitation in terms of solute diffusion, excess vacancy annihilation, vacancy trapping and repartitioning. Then, we show that this model based on parameters taken from first-principles calculations represents the experimental characteristics during isothermal ageing (Section 4.2) and linear heating after various pre-ageing treatments (Section 4.3) very well. Finally, we demonstrate that the effect of natural pre-ageing on the DSC cluster peak can be described by including vacancy trapping by solute clusters into the model (Section 4.4).

4.1. Model

In order to relate the course of vacancy site fraction under a given applied temperature profile to the state of precipitation we apply a simple model based on the following assumptions:

1. The precipitated state is represented by a single variable $\alpha \in [0, 1]$, the fraction of clusters/precipitates formed without specifying details of size, distribution, composition, etc. (N.B. as customary we call a precipitate in an early stage at which it still has the structure of the parent lattice a 'cluster').
2. All the vacancies are considered to be mono-vacancies. Formation of structures containing more vacancies is neglected.
3. Solute atoms transfer from the solid solution to other solutes or clusters as they diffuse through the lattice and attach to them while the remaining solutes are still distributed homogeneously.
4. Once clusters/precipitates have formed, they do not dissolve. Thus, α always increases.

4.1.1. Precipitation

From the initially N^i_{tot} solute atoms of type $i \in$ {Mg, Si, ...}, we subtract the already clustered solutes N^i_{cl} and write for the progress of clustering in a time interval dt

$$dN^i_{\text{cl}} = \left(N^i_{\text{tot}} - N^i_{\text{cl}}\right) \cdot N^i_{\text{vis}}(dt) \cdot p_{\text{att}}, \tag{1}$$

where dN^i_{cl} scales with the number of sites $N^i_{\text{vis}}(dt)$ a solute on its random walk visits in time dt and the probability p_{att} for a solute atom to encounter target sites (around solutes, clusters) and be actually absorbed there.

In the five frequency model of diffusion [26] the frequency of solute-vacancy exchanges for component i is $w^i_2 = \nu^{*,i}_2 \cdot e^{-\frac{\Delta H^i_{m,2}}{kT}}$, with $\nu^{*,i}_2$ and $\Delta H^i_{m,2}$ the effective vibrational frequency and migration enthalpy change for the exchange (index 2). The number of sites visited by a solute equals the number of successful jumps multiplied by the probability of jumping to a new site:

$$N^i_{\text{vis}}(dt) = f^i_2 \cdot \nu^{*,i}_2 \cdot e^{-\frac{\Delta H^i_{m,2}}{kT}} \cdot z \cdot x^i_{v,trp}(T,t) \cdot dt, \tag{2}$$

with $x^i_{v,trp}(T,t)$ the probability of finding a vacancy temporarily trapped at one of the nearest neighbour sites of solute i, which is a condition for solute jumping, $z = 12$ the fcc coordination number, f^i_2 the correlation factor (which depends on the other four jump frequencies) expressing that a solute might jump back to its previous position. By combining Eqs. (1, 2) and defining $\alpha^i = \frac{N^i_{\text{cl}}}{N^i_{\text{tot}}}$, we obtain

$$\frac{d\alpha^i}{dt} = p_{\text{att}} \cdot z \cdot \left(1 - \alpha^i\right) \cdot \underbrace{f^i_2 \cdot \nu^{*,i}_2 \cdot e^{-\frac{\Delta H^i_{m,2}}{kT}}}_{M^i} \underbrace{x^i_{v,trp}(T,t)}_{V^i}, \tag{3}$$

M^i, V^i are used in the further discussion. In equilibrium, the impurity diffusion coefficient is given by $D^i_2 = a^2 M^i V^i$, with a the lattice constant [27]. The various kinds of solutes i, concentrations c^i, precipitate simultaneously and define a total α:

$$\frac{d\alpha}{dt} = \frac{1}{\sum_i c^i} \sum_i c^i \frac{d\alpha^i}{dt}. \tag{4}$$

p_{att} takes account of the probability of the diffusing solute to be at a site that neighbours a target and attaching to it. Both solute atoms and clusters can be such targets. Initially, the site fraction of attachment sites is the highest but the attachment rate might be low due to weak binding. As solutes are consumed and clusters increase in size, the attachment sites decrease in numbers, while the success rate might increase due to stronger binding. p_{att} is hard to model without introducing many parameters, which would obscure the message we intend to convey. Therefore, we assume that for a given alloy, p_{att} is constant throughout clustering in the temperature interval of interest to allow us to focus on the behaviour of excess vacancies, see also supplement S3. The value used in this work is chosen such that the first peaks of the hardening curves in (Fig. 1b) and DSC experiments (Fig. 2a) are reproduced and reach roughly 1/3 of the height of the second peak.

4.1.2. Excess vacancy annihilation

In pure Al, the equilibrium vacancy site fraction at temperature T is:

$$x_{v-eq} = e^{-\frac{\Delta G_{f,0}}{kT}}, \tag{5}$$

where $\Delta G_{f,0}$ is the vacancy formation Gibbs free energy. When vacancies are in excess, $x_v(T,t)$ depends on time and vacancy annihilation has to be treated. We assume that vacancies primarily annihilate at grain boundaries of spherical grains, radius R, and dislocation jogs, number density n_{jog}, free of hydrostatic stress. The rate of annihilation, i.e. change of $x_v(T,t)$, is given by [28]:

$$\frac{dx_v}{dt} = -\left(\frac{15}{R^2} + 2\pi a n_{\text{jog}}\right) \frac{\tilde{D}_{eq}}{f_0} \frac{x_v}{x_{v-eq}} \ln\left(\frac{x_v}{x_{v-eq}}\right), \tag{6}$$

with a the lattice constant and $\tilde{D}_{eq}(T)$ the concentration-weighted diffusion coefficient of solvent, $D_0(T)$, and solute atoms, $D^i_2(T)$. f_0 is the fcc correlation factor (=0.7815).

4.1.3. Vacancy trapping and repartitioning

x_{v-eq} in Eq. (5) represents the site fraction of vacancies in a pure lattice. In the presence of solute atoms, the probability of finding a vacancy 'trapped' in the shell around a solute atom i is modified due to its binding energy ΔG^i_b ('+' denotes attractive binding) with the solute and we obtain two different vacancy fractions around the solute (index '*trp*') and in the matrix (index '*mat*') [29]:

$$x_{v-eq}(T) = \left(1 - (1+z)\sum_i c^i\right) \underbrace{e^{-\frac{\Delta G_{f,0}}{kT}}}_{x_{v-eq,mat}} + z \sum_i c^i \underbrace{e^{-\frac{\Delta G_{f,0}}{kT}} \cdot e^{\frac{\Delta G^i_b}{kT}}}_{x^i_{v-eq,trp}}, \tag{7}$$

This 'Lomer equation' is a special case of more general equations that also include strong trapping and multi-vacancy complexes [30]. They can be inverted to express $x^i_{v,trp}(T,t)$ by the total vacancy site fraction $x_v(T,t)$ also in non-equilibrium (see supplement S2):

$$x^i_{v,trp}(T,t) = \frac{e^{\frac{\Delta G^i_b}{kT}}}{1 - (1+z)\sum_i c^i + z\sum_i c^i e^{\frac{\Delta G^i_b}{kT}}} x_v(T,t), \tag{8}$$

The solute fractions c^i in Eqs. (7, 8) will change as precipitation progresses and solutes are confined in precipitates. We will discuss later that accounting for this quantitatively is not necessary.

The quantities in Eq. (7) have to be used in Eq. (6) to account for vacancy trapping by solutes (but not trapping by clusters). We will include trapping by clusters in Section 4.4 and present the modifications to Eq. (8) along with a detailed derivation in supplement S2. Vacancy trapping and repartitioning by solutes or clusters has been tacitly assumed to be instantaneous as the diffusion of vacancies to the traps (sites adjacent to solutes) requires just short-range displacements in contrast to diffusion to more distant sinks [30].

4.1.4. Calculations

Numerical integration starts from initially $\alpha = 0$ and $x_v(T,t) = x_{v-eq}(540°C)$ using Eq. (7). For each time increment dt, $x_v(T,t)$ is updated using Eq. (6), after which Eq. (8) is used to obtain $x^i_{v,trp}(T,t)$, which is put into Eqs. (3, 4) to determine $d\alpha$. Our simulation of vacancy loss and solute migration is based on a published set of parameters calculated by first principles for Mg and Si solutes in Al using density functional theory and the local density approximation [31]. The advantage over referring to experimental values for the various energies and entropies involved is that such calculated data are consistent. The parameters used are listed in supplement S1. Diffusion of the small amount of Cu present in the real alloy is neglected since its influence is very small, see supplementary Fig. S6.

In comparing $\alpha(t)$ to experimental data we have to make some further assumptions. The first is, that the heat flow during ageing is proportional to the derivative of $\alpha(t)$. This implies that the enthalpy of cluster formation is proportional to its volume only and not to other parameters such as surface area, cluster composition or strain energy. Furthermore, we assume that $\alpha(t)$ is proportional to the hardness increase during ageing. This is a reasonable approximation for cluster hardening as experiments for alloy 6014 [32] and calculations [33] have shown, but not for precipitate hardening. The latter involves various different phases and complex diffusional transformations that possibly require more than one acting vacancy at a time [34]. Moreover, due to a different strengthening mechanism the relationship between strength and precipitated volume is no longer linear [35,36]. We can therefore not expect to model the details of hardening correctly for higher temperatures, which is not our objective anyway. The fact that real DSC traces exhibit 2 or more peaks at high temperatures (see Fig. 2b), our calculation just one (see below) shows this limitation.

In thermal equilibrium our precipitation model in Eq. (3) takes the form of a Johnson-Mehl-Avrami-Kolmogorov (JMAK model) with an Avrami index equal to 1, which is just a special case of a more general class of rate equations [37].

4.2. Simulation of isothermal ageing

We apply isothermal treatments between −60 °C and 200 °C after solutionising at 540 °C and quenching at 1000 $K \cdot s^{-1}$. Fig. 4a presents vacancy site fractions at Mg and Si sites from Eq. (8) as they evolve at 20 °C. As only Si has an attractive vacancy-solute interaction (>0) within the parameter set used (the interaction energy V−Mg is <0 here in variance to most of the literature [38-42] but in accordance to Ref. [43]), the site fraction around Si atoms is much higher, which contributes to faster diffusion of Si. Initially, vacancies are continuously lost, but as lower temperatures are reached during quenching, the trapping effect at Si sites increases in strength and vacancies from the matrix repartition and let $x^{Si}_{v,trp}$ increase again. Equilibrium site fractions are reached after about 5×10^5 s (6 days).

Fig. 4b shows how the precipitated fraction α and its derivative evolve at 20 °C and 60 °C. At the higher temperature, clustering is faster, but the α eventually reached is lower. This can be understood by looking at the derivative of α, which is essentially the product of the vacancy (V) and the migration (M) terms in Eq. (3). At 60 °C, $d\alpha/dt$ has dropped to 1% of its initial value after 1600 s (red arrow) and α has almost reached a saturation value (red broken line), whereas for 20 °C it takes just about 6 times longer to reach the same level of α (blue broken line) although the migration term M in Eq. (3) is 13 times lower for 20 °C than for 60 °C. The reason is that the vacancy site fraction remains at a reasonably high level for a much longer time due to slower annihilation (see inset). The increase of α at 20 °C continues after and although the vacancy site fraction drops the long available time allows for a further increase until after 40000 s α levels off at a level not reached at 60 °C.

Ageing eventually goes through a second step for longer times than shown in Fig. 4b. Fig. 4c demonstrates this for isothermal ageing at various temperatures. For even longer times than shown there, α increases to 1 for any temperature purely driven by equilibrium vacancies. At 20 °C it takes 10^{11} s to complete ageing (curve truncated at $10^6/10^8$ s in Figs. 4b/c), which of course is not observable in experiments where we always measure just the first stage. In Fig. 4c, the times at which excess vacancies are exhausted are marked by symbols on each curve. We see that for any ageing temperature ≤100 °C, the first ageing step driven by excess vacancies is more pronounced for lower temperatures, whereas the second step that takes place in thermal equilibrium strictly follows the expected kinetics, i.e. faster and higher α for higher temperatures. Note that not only hardness but also electrical resistivity increases faster at lower temperatures [16,17], which could have similar reasons.

Fig. 4d displays ageing curves for different times as a function of temperature. This result has to be compared to Fig. 1b. The simulation obviously represents the main stages of the experiments very well with the exception of stage IV (overageing) that is not included in the model. The observed maxima and minima of the experimental curve and stage II in Fig. 1b are well reproduced by the simulation as shown for example for 4 h of ageing by arrows. If one differentiates in Eq. (3) between equilibrium and excess vacancy contributions by using either $x^i_{v-eq,trp}(T)$ or $x^i_{v,trp}(T) - x^i_{v-eq,trp}(T)$ for the last term V^i there, respectively, we obtain the black broken lines for 10 min ageing time, $\alpha_{ex}(T)$ and $\alpha_{eq}(T)$, and see that below ~125 °C all precipitation within 10 min is driven by excess vacancies. For any ageing time the excess vacancy contributions merge into the black broken line. These simulations therefore clearly underline that the two hardening regimes in Fig. 1b can be associated to a regime of excess vacancy driven clustering and a second high-temperature regime governed by equilibrium vacancies. The differences between Fig. 4d and Fig. 1b (e.g. ageing time dependence of hardness in stage II) indicate that nucleation effects or different strengthening efficiencies of precipitates formed at different temperature might also play a role. Fig. S1 of the supplement shows data in addition to Fig. 4d with adjustments of the concentrations c^i in Eqs. (7, 8) taken into account. The effect of such adjustments is very small.

4.3. Simulation of linear heating

We apply a linear heating profile after solutionising and quenching and obtain from Eqs. (3, 4) the 'DSC trace', i.e. the derivative of α, for the two components and the total. Fig. 5 features two peaks as T increases, the first at ~75 °C, the second at ~250 °C, which is in accordance with the clustering and precipitation peaks in the experimental DSC curves, Fig. 2a,b. The relative heights of the two peaks are the same in the calculations and the experiment. For temperatures below 200 °C, precipitation of Si dominates, which is why we use the vacancy site fraction $x^{Si}_{v,trp}$ to explain the effects. It exhibits a minimum between the two peaks, demonstrating that the first peak correlates with a large excess of

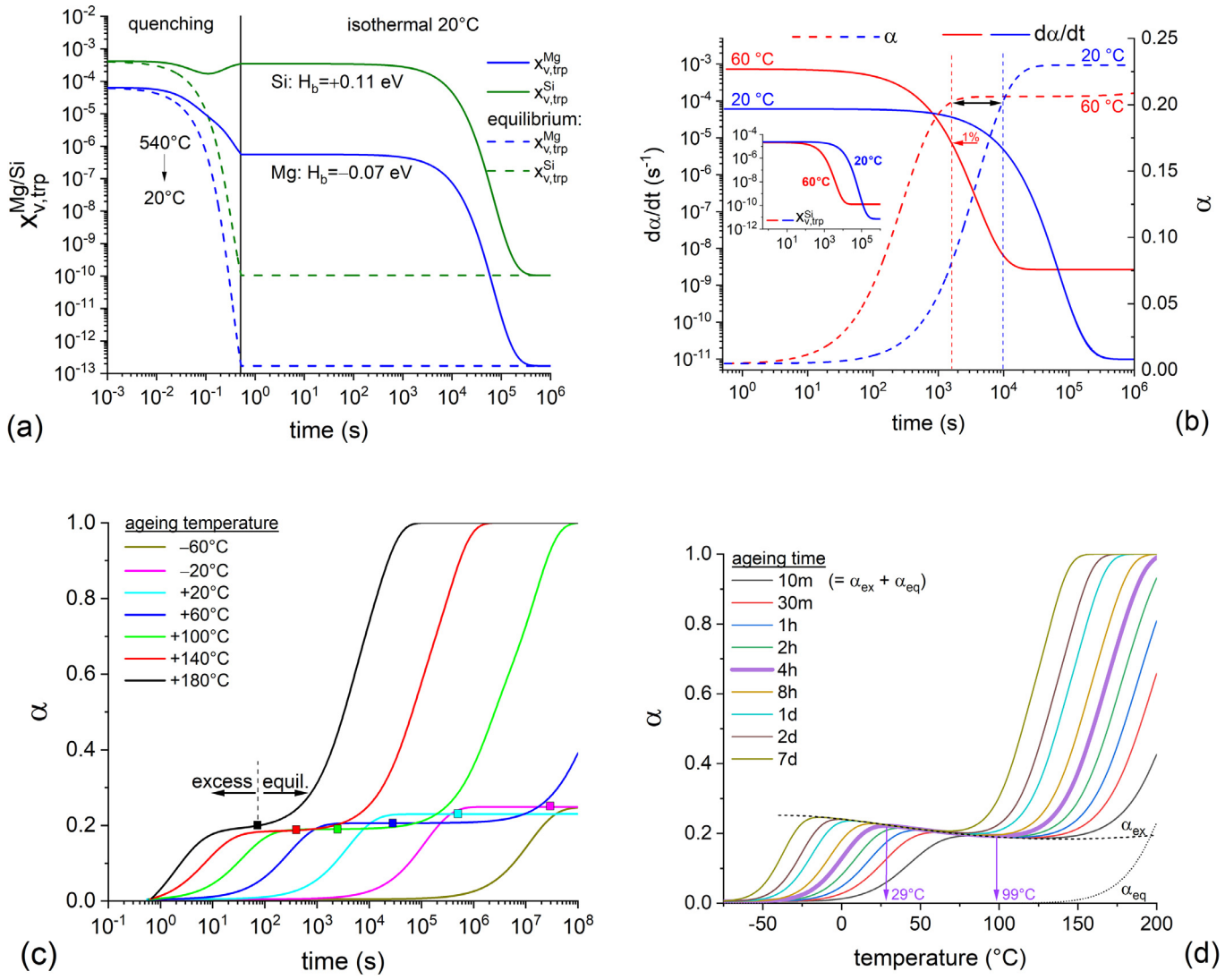

Fig. 4. Calculated isothermal ageing after solutionising and quenching in alloy 6014. a) Course of local vacancy site fractions around Mg and Si atoms and the corresponding equilibrium values. b) α and $d\alpha/dT$ during isothermal ageing at 20 °C and 60 °C demonstrating higher achievable excess-vacancy driven precipitation at the lower temperature (arrows and lines explained in the text, inset shows course of vacancy Si-site fraction). c) Isothermal ageing at different temperatures driven mainly by excess vacancies left of each square on a curve, by equilibrium vacancies right of each square. (d) Ageing for different times displayed as a function of ageing temperature. For 10 min ageing time, the curve has been decomposed into ex(cess), α_{ex}, and eq(uilibrium), α_{eq}, contributions. The excess vacancy contribution is the same for all ageing times at high temperatures and has been continued towards lower temperatures (dashed line).

vacancies, the second with equilibrium vacancies. The product of the vacancy fraction and the Si migration enthalpy – V^{Si} and M^{Si} in Eq. (3) – is responsible for the first peak. At low temperatures, say −20 °C, the migration term is too low to allow for clustering, whereas around 130 °C annihilation of excess vacancies limits further clustering. The re-increase of the equilibrium vacancy site fraction and the faster migration then give rise to the second peak which comes to an end because α eventually approaches 1. The high-temperature range is also influenced by $x^{Mg}_{v,trp}$ as seen from the Mg-related peak. Mg might gain additional influence via interactions with other elements even at 'room temperature' as shown for example for Al-Cu-Li alloys [44] but this is beyond the model used here.

If samples are aged at 180 °C before DSC, the simulated peak is modified, see Fig. 6a. Ageing for up to 30 s completely eliminates the first peak. The primary reason is that excess vacancies anneal out and not so much because solute is consumed (see inset). In 10 s of AA the vacancy site fraction around the Si atoms is reduced from 450 times to just about 15 times the equilibrium value at 180 °C (see inset), which has a very pronounced effect. In contrast, in 10 s of AA, just a small fraction of the available solutes are consumed. The calculated DSC curves in Fig. 6a correspond very well to Fig. 2a including the slight shift of the peak maximum to higher temperatures (short broken line), and Fig. 6b represents Fig. 2d very well. After about 100 s of AA, the second peak in Fig. 6a also starts to decrease. As we are dealing exclusively with equilibrium vacancies at this stage, the reason is solute consumption during AA preceding DSC. This fits nicely to the experimentally observed onset of AA after 2 min, see Fig. 1a.

4.4. Simulation of vacancy trapping by clusters

NA influences the DSC trace in a different way than AA, see Fig. 2c,e, and we suspect that is due to interactions between vacancies and clusters. In order to verify this, we carried out calculations including trapping of vacancies by clusters. The Lomer equation can be extended to trapping of vacancies by small clusters if they are thought to be point-like, see supplement Eq. (S10). Unlike solute atoms, clusters do not contribute to diffusion in Eq. (6). We

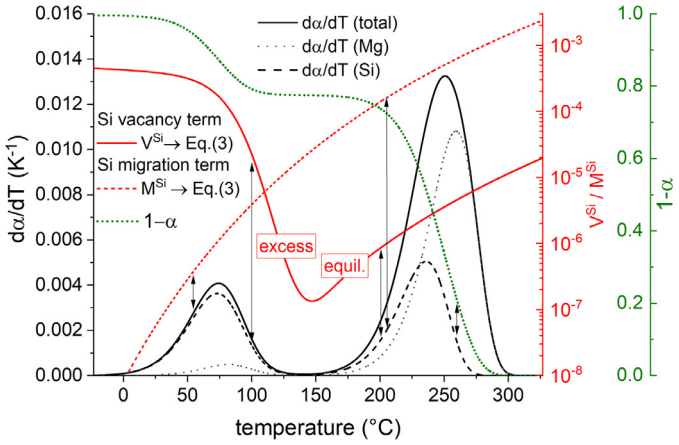

Fig. 5. Calculated $d\alpha/dT$ ('DSC trace'), heating rate 10 K·min^{-1} (black). Red lines show the local vacancy site fraction around Si atoms – term 'V' in Eq. (3) –, the broken line the Si migration term labelled 'M' in Eq. (3) (re-scaled to approximately match V). The corresponding data for Mg has been omitted since clustering is dominated by Si diffusion up to ~200 °C as seen by the decomposition of $d\alpha/dT$ into Mg and Si contributions. The vertical arrows relate the changes of the DSC curve to the quantities that have the largest influence.

assume that vacancies interact stronger with clusters than with individual solutes, a viewpoint recently confirmed by calculations of the binding of a vacancy and two solute atoms [39]. Further recent calculations have shown typical interaction energies ranging from 0.306 eV for small clusters formed by short NA to 0.581 eV for an advanced NA state in more concentrated alloys [45]. Atom probe measurements suggest cluster number densities of typically 10^{23}-10^{24} m^{-3} [4,46,47] (possibly missing out very small clusters), while positron lifetime experiments rather yield 10^{25} m^{-3} [21]. With this in mind, we assume that the cluster number density increases linearly from 0 to 6×10^{24} m^{-3} (site fraction c^{cl} from 0 to 10^{-4}) as α goes from 0 to 1. For the vacancy-cluster interaction energy ΔH_b^{cl} we use values of 0.2 eV for the first clusters (which is more than between a vacancy and a single Si atom, 0.11 eV), 0.306 eV for short NA (α=0.2) and 0.581 eV for long NA. This leads to the linear parametrisation $\Delta H_b^{cl} = 0.2 + 0.53 \times \alpha$ [eV]. It is less rigorously based on calculated data and an elaborate model than the ones in the previous sections but appears a reasonable approach to estimate the effect of vacancy-cluster interactions.

Fig. 7a shows the effect of trapping on NA that is delayed towards higher ageing times. This is due to increasing vacancy trapping by clusters that are formed during NA – caused by the increase of the interaction energy and cluster fraction with α. The shape of the curve deviates from that of a JMAK model even with different values of the Avrami index n. This is related to the difficulties encountered when trying to fit hardness or resistivity data to JMAK-type functions [19,48], namely that experimental NA hardening curves tend to be flatter in later stages than the most reasonable JMAK fit. The current authors, for example, found that hardness during NA evolves more like the red than the black line in Fig. 7a [19].

Next, the effect of vacancy trapping is investigated for linear heating both after ageing at 180 °C and NA as shown in Fig. 2c,e. The effect is very different in the two cases: While the course of the rate of clustering ('DSC trace') is only moderately altered for AA (compare Fig. 6a and Fig. 7b), a more notable shift is obtained for NA (Fig. 7c). To make this more visible, Fig. 7d compares the peak positions and heights for the data given in Fig. 6a and data calculated for NA without cluster trapping (not shown) with the data in Fig. 7b,c (trapping by clusters). In the latter case, NA before linear heating shifts the DSC peak by more than 60 K for the longest ageing time. The DSC curve in Fig. 7c resembles the experimental curve Fig. 2e very closely. Thus, these simulations underline the importance of vacancy-cluster interaction in simulating some experimental observations.

5. Discussion

The quenched microstructure of an alloy contains a high solute supersaturation and excess vacancies, which both tend to be reduced towards the equilibrium state during ageing. The ageing temperature as the key parameter determines the kinetics of the processes, more specifically the rates of cluster formation and vacancy evolution, and especially the role of the excess vacancies in accelerating solute diffusion. We have demonstrated experimentally and with simulations that, as the ageing temperature varies, cluster formation is a result of a competition between excess vacancy annihilation and the diffusion process, both thermally activated. It is shown that NA primarily benefits from excess vacancies that survive for a long time. In contrast, they are largely removed in the initial seconds of AA without causing much hardening. Therefore, most of AA can be attributed to equilibrium va-

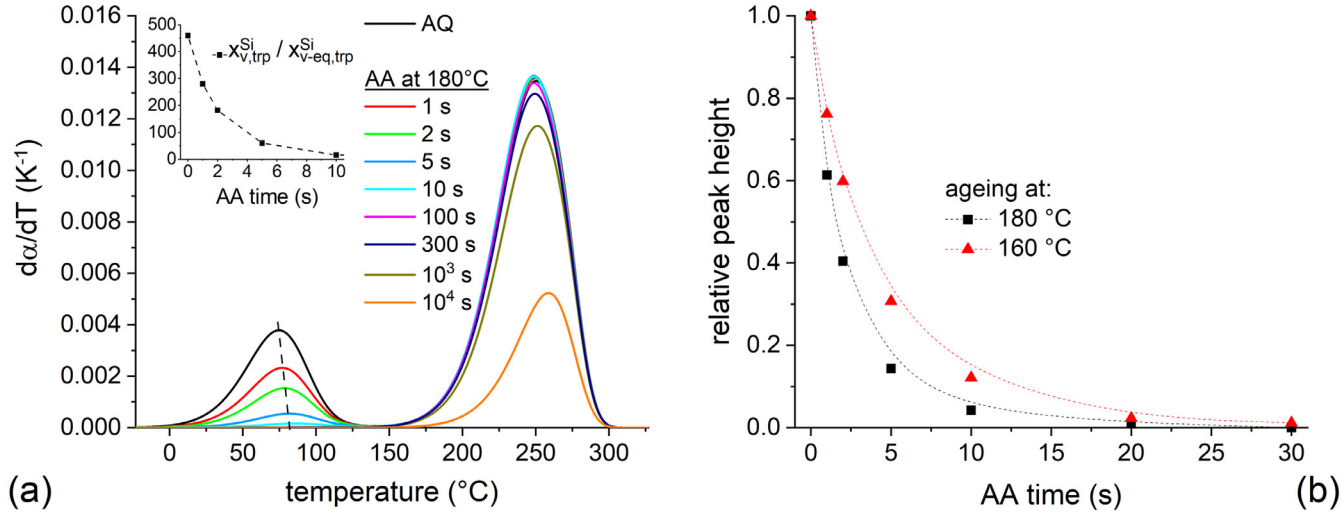

Fig. 6. (a) Calculated $d\alpha/dT$ ('DSC trace'), heating rate 10 K·min^{-1} for as-quenched samples (AQ) and samples aged at 180 °C (AA) prior to DSC. Inset: vacancy site fraction $x^{Si}_{v,trp}$ relative to equilibrium value at 180 °C before the DSC run. (b) Height of clustering peak for samples aged at 180 °C and 160 °C relative to peak height in AQ sample.

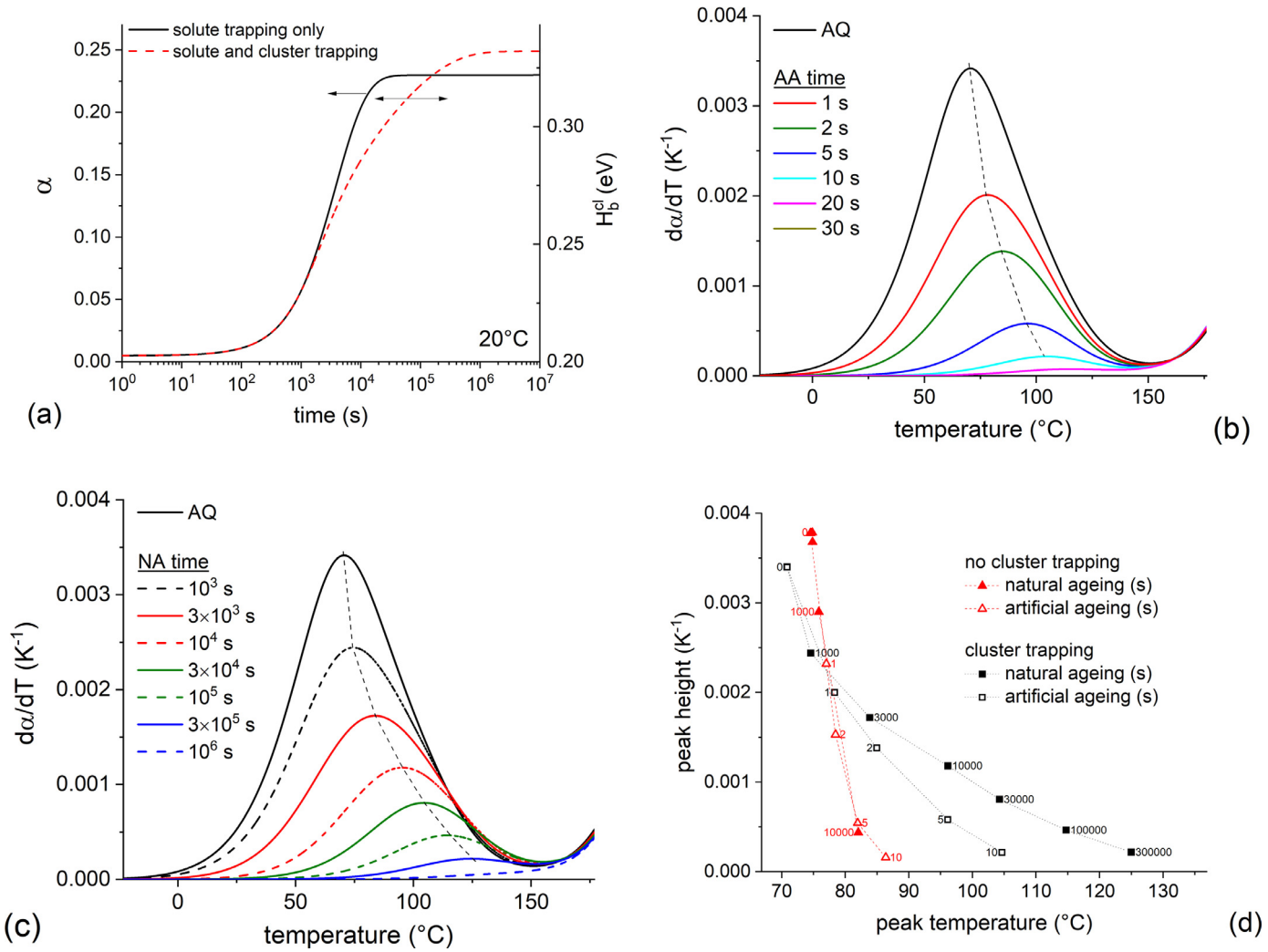

Fig. 7. Effect of trapping of vacancies by clusters. (a) NA at 20 °C in comparison to simulation without cluster trapping, (b) Heating at 10 K·min^{-1} after short ageing at 180 °C (AA), (c) Heating at 10 K·min^{-1} after NA at 20 °C, (d) comparison of peak heights and positions for the 4 scenarios studied (from Figs. 6a, 7b and 7c and one not shown).

cancies and the fast kinetics originate from the pronounced thermal activation of solute diffusion. In the intermediate temperature regime, however, the faster increase of vacancy annihilation than of solute migration with higher temperature results in the observed hardening anomaly in stage II of Fig. 1b, i.e. higher ageing temperature results in lower hardening for a given time. In the following, we further discuss the mechanism that controls this phenomenon and discuss how it might be utilised to help designing better heat treatment strategies.

5.1. Mechanisms controlling the competing processes

Both the annihilation of excess vacancies and solute diffusion rely on the same physical process—vacancy jump. At higher temperature, the equilibrium vacancy site fraction is reached faster due to a higher vacancy jump frequency. However, on the way to the sinks, excess vacancies also transport solute atoms when they exchange positions with them. Therefore, how fast excess vacancies reach sinks —determined also by the vacancy sink density— should not be the underlying cause of the hardening anomaly, because solute diffusion is influenced accordingly. It has to be that fewer *total* solute jumps occur at higher ageing temperature as excess vacancies annihilate out, i.e. vacancies are less efficient in assisting solutes to jump. This can be understood by calculating the total clustered fraction caused by the excess vacancies only (dashed line $\alpha_{ex}(T)$ in Fig. 4d). To obtain an analytical expression for this line, we simplify the scenario and do not consider vacancy trapping by clusters and perform the calculation with only one solute element, namely Si, since it is the main diffuser at low temperature (Fig. 5). An analytical solution can be conveniently given for the integration of Eqs. (3–8) at isothermal ageing conditions. The detailed calculation can be found in supplement S4. The simplified final result is:

$$\alpha_{ex}(T) = 1 - e^{\left[-B\ \frac{D_2(T)}{\tilde{D}_{eq}(T)}\ \zeta(T)\right]} \tag{9}$$

where B is a positive temperature-independent term, and $\zeta(T)$ is a slowly increasing function of temperature which is related to the model in Eq. (6) (the exponentially decaying excess vacancy model used in [49,50] does not contain this term). The average and solute diffusion coefficients $\tilde{D}_{eq}(T)$ and $D_2(T)$ have been defined above. Fig. 8a shows all temperature dependent terms in Eq. (10). The decreasing $\alpha_{ex}(T)$ in the temperature range of interest is due to a decreasing $\frac{D_2}{\tilde{D}_{eq}}$. Since $\tilde{D}_{eq}$ can be approximated by the solvent diffusion coefficient $D_0(T)$ in this temperature range, the reason for the decreasing $\alpha_{ex}(T)$ can be attributed to a lower migration activation energy of D_2 than D_0. In other words, the hardening anomaly is caused by the competition between solute diffusion and self-

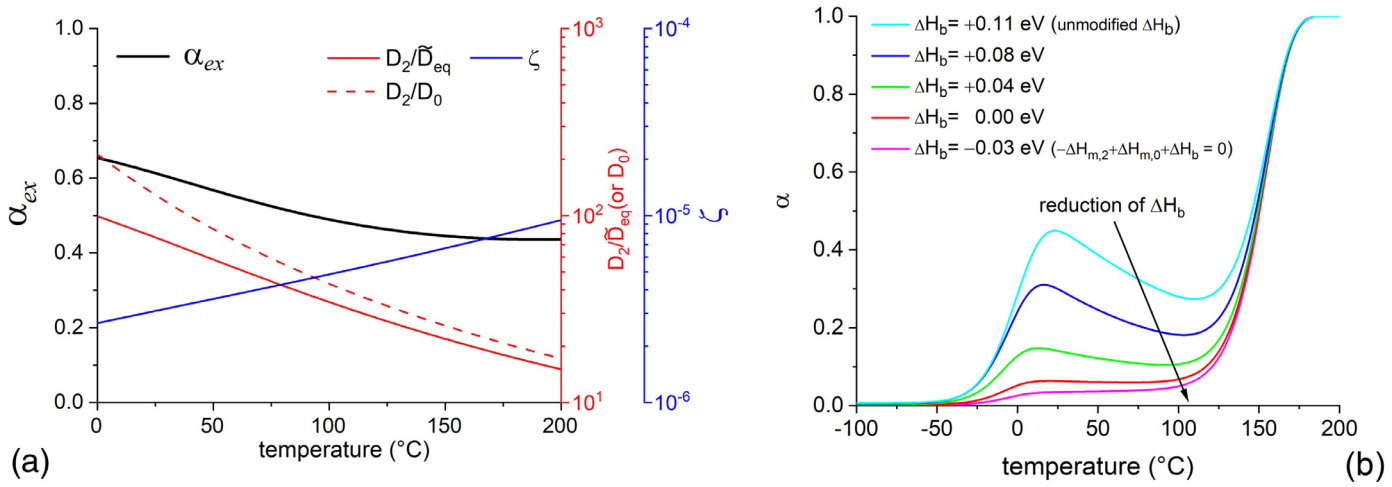

Fig. 8. Discussion of the origin of the hardening anomaly. (a) Temperature-dependent factors in Eq. (9) causing the anomaly. (b) Precipitation after 4 h of ageing as a function of temperature. Lines from top to bottom: stepwise decrease of ΔH_b^{Si} from the original value of 0.11 eV down to −0.03 eV, while ensuring that $\Delta H_{f,0} - \Delta H_b^{Si} = 0.6$ eV = const. The anomaly, i.e both maxima and minima, gradually disappears. In both graphs, only Si diffusion is taken into account.

diffusion. To demonstrate this conclusion, we can vary $\frac{D_2}{D_0}(T)$ and observe the influence on the hardening anomaly. By writing [31]:

$$\frac{D_2}{D_0} = \frac{f_2}{f_0}\frac{\nu_2^*}{\nu_0^*} e^{\frac{-\Delta H_{m,2}+\Delta H_{m,0}+\Delta H_b}{kT}} e^{\frac{-\Delta S_b}{k}}, \quad (10)$$

with symbols as in Eqs. (3, 7) and in Table S1 of the supplement, we can manipulate the hardening anomaly by changing ΔH_b and letting the sum of the 3 enthalpies go to zero (one could also manipulate $\Delta H_{m,2}$, $\Delta H_{m,0}$, or f_2). Fig. 8b shows that by reducing ΔH_b from 0.11 eV to −0.03 eV, we gradually remove the temperature dependence of $\frac{D_2}{D_0}(T)$ and thus also the hardening anomaly.

Since all the simulation results depend on the input data used, a consistent parameter set is crucial for the simulation. The parameters provided by Ref. [31] are consistent and reproduce real diffusion data, which is why they are adopted in this work. However, the conclusions obtained should be still valid if other parameter sources are used as long as they fulfill the same criteria.

To illustrate the robustness of the current approach supplementary Fig. S5 shows the consequence of changing the vacancy-Mg binding energy to a positive value as claimed by various sources [38-42]. It is seen that the conclusions of this paper can all be held despite such changes.

5.2. Implication for industrial application

Understanding the role of excess vacancies and their interplay with precipitation helps in designing improved heat treatments. For instance, for the currently studied 6xxx alloys that are widely used as car body panel materials, storage in the low-strength state is required to ensure good formability before stamping. Therefore, alloys are normally pre-aged at intermediate temperature to anneal out excess vacancies without too much hardening to ensure slow hardening during subsequent natural secondary ageing [18]. Excess vacancies might be useful in other cases since hardening at low temperature for the same time can be as effective as ageing at higher temperatures. This could significantly reduce the energy consumption by replacing high-temperature ageing by low-temperature or even room temperature ageing if possible. To further enhance hardening at low temperatures requires even more vacancies, which might be provided by continuous straining of the material [50,51].

6. Conclusions

The role of quenched-in excess vacancies during age hardening at various temperatures in an Al-Mg-Si aluminium alloy has been investigated using various experimental methods (hardness, DSC, positron lifetime measurements) and precipitation simulations with the consideration of excess vacancy annihilation. We find:

- After AA even for just a few seconds, the cluster peak in the DSC trace disappears and the positron lifetimes drops markedly, evidencing that excess vacancies are largely removed.
- Hardening curves as a function of temperature for various isotimes show a double peak structure, which divides the curves into four stages. The peak at lower temperature is primarily caused by excess vacancies and the one at higher temperature by equilibrium vacancies. Of particular interest is the inter-peak region ('stage II') where an increasing temperature leads to a stronger vacancy loss that outruns the enhanced thermal activation of precipitation. As a consequence, slower hardening is obtained despite the higher temperature.
- Simulations based on a realistic treatment of vacancy evolution and ab-initio diffusion parameters, reproduce the experimental features of isothermal ageing at various temperatures as well as linear heating (DSC) after AA very well. The shift of the DSC cluster peak after NA can be simulated by implementing a less rigorous vacancy-cluster interaction model.

All these results suggest that NA is a process that is governed by excess vacancies while AA is caused by equilibrium vacancies except for a very short initial period. The hardening difference caused by excess vacancies at different temperatures can be attributed to the competition between excess vacancy annihilation and solute precipitation, which is governed by a ratio between the solute- and self-diffusion coefficients. Understanding the role of excess vacancies in ageing might allow the industry to engineer more efficient heat treatments, especially because the basic mechanisms discovered here can also be applied to other alloys.

Declaration of Competing Interest

The authors declare that they have no known competing financial interests or personal relationships that could have appeared to influence the work reported in this paper.

Acknowledgements

We are grateful to Novelis R&D Centre in Sierre for providing alloy samples.

Supplementary materials

Supplementary material associated with this article can be found, in the online version, at doi:10.1016/j.actamat.2021.117014.

References

[1] J. Hirsch, Annealing of aluminium and its alloys, in: G.E. Totten, D.S. MacKenzie (Eds.), ASM Handbook, Vol 4E: Heat treating of nonferrous alloys, ASM International, Materials Park, OH (USA), 2016, pp. 137–147.
[2] J. Banhart, M.D.H. Lay, C.S.T. Chang, A.J. Hill, Kinetics of natural aging in Al-Mg-Si alloys studied by positron annihilation lifetime spectroscopy, Phys. Rev. B 83 (2011) 014101.
[3] M. Saga, Y. Sasaki, M. Kikuchi, Z. Yan, M. Matsuo, Effect of pre-aging temperature on the behavior in the early stage of aging at high temperature for Al-Mg-Si alloy, Mater. Sci. Forum 217 (1996) 821–826.
[4] M.W. Zandbergen, Q. Xu, A. Cerezo, G.D.W. Smith, Study of precipitation in Al-Mg-Si alloys by atom probe tomography I. Microstructural changes as a function of ageing temperature, Acta Mater. 101 (2015) 136–148.
[5] M. Torsæter, H.S. Hasting, W. Lefebvre, C.D. Marioara, J.C. Walmsley, S.J. Andersen, R. Holmestad, The influence of composition and natural aging on clustering during preaging in Al-Mg-Si alloys, J. Appl. Phys. 108 (2010) 073527.
[6] A. Poznak, R.K.W. Marceau, P.G. Sanders, Composition dependent thermal stability and evolution of solute clusters in Al-Mg-Si analyzed using atom probe tomography, Mater. Sci. Eng. A 721 (2018) 47–60.
[7] S. Pogatscher, H. Antrekowitsch, H. Leitner, D. Poschmann, Z.L. Zhang, P.J. Uggowitzer, Influence of interrupted quenching on artificial aging of Al-Mg-Si alloys, Acta Mater. 60 (2012) 4496–4505.
[8] J.D. Bryant, The effects of preaging treatments on aging kinetics and mechanical properties in AA6111 aluminum autobody sheet, Metall. Mater. Trans. A 30A (1999) 1999–2006.
[9] A. Lutts, Pre-precipitation in Al-Mg-Ge and Al-Mg-Si, Acta Metall. 9 (1961) 577–586.
[10] K. Yamada, T. Sato, A. Kamio, Effects of quenching conditions on two-step aging behavior of Al-Mg-Si alloys, Mater. Sci. Forum 331-337 (2000) 669–674.
[11] W. Desorbo, H.N. Treaftis, D. Turnbull, Rate of clustering in Al-Cu alloys at low temperatures, Acta Metall. 6 (1958) 401–413.
[12] F. Federighi, Quenched-in vacancies and rate of formation of zones in aluminum alloys, Acta Metall. 6 (1958) 379.
[13] S. Esmaeili, D.J. Lloyd, Effect of composition on clustering reactions in AlMgSi(Cu) alloys, Scripta Mater. 50 (2004) 155–158.
[14] C. Haase, H. Wurst, Zur Frage der Kalt- und Warmaushärtung bei Aluminium-Magnesium-Silizium-Legierungen, Zeitschrift für Metallkunde 33 (1941) 399–403.
[15] A. Durer, W. Köster, Beitrag zur Frage der Kalt- und Warmaushärtung auf Grund thermoelektrischer Untersuchungen, Zeitschrift für Metallkunde 30 (1938) 311–319.
[16] C. Panseri, T. Federighi, A resistometric study of preprecipitation in an aluminium-1.4% Mg_2Si alloy, J. Inst. Metal. London 94 (1966) 99–197.
[17] I. Kovács, J. Lendvai, E. Nagy, The mechanism of clustering in supersaturated solid solutions of Al-Mg_2Si Alloys, Acta Metallurgica 20 (1972) 975–983.
[18] Z. Yang, Z.Q. Liang, D. Leyvraz, J. Banhart, Effect of pre-ageing on natural secondary ageing and paint bake hardening in Al-Mg-Si alloys, Materialia 7 (2019) 100413.
[19] Z. Yang, X.H. Jiang, X.-P. Zhang, M. Liu, Z.Q. Liang, D. Leyvraz, J. Banhart, Natural ageing clustering under different quenching conditions in an Al-Mg-Si alloy, Scripta Mater. 190 (2021) 179–182.
[20] M. Madanat, M. Liu, X.-P. Zhang, Q.-N. Guo, J. Cizek, J. Banhart, Co-evolution of vacancies and solute clusters during artificial ageing of Al-Mg-Si alloys, Phys. Rev. Mater. 4 (2020) 063608.
[21] M. Liu, J. Čížek, C.S.T. Chang, J. Banhart, Early stages of solute clustering in an Al–Mg–Si alloy, Acta Mater. 91 (2015) 355–364.
[22] J.M. Silcock, The structural ageing characteristics of Al-Cu-Mg alloys with copper-magnesium weight ratios of 7-1 and 2.2-1, J. Inst. Metal. Lond. 89 (1960) 203–210 -61.
[23] I.J. Polmear, The ageing characteristics of ternary aluminium-zinc-magnesium alloys, J. Inst. Metal. 86 (1957) 313–321 -58.
[24] G.A. Edwards, K. Stiller, G.L. Dunlop, M.J. Couper, The precipitation sequence in Al-Mg-Si alloys, Acta Mater. 46 (1998) 3893–3904.
[25] A.K. Gupta, D.J. Lloyd, Study of precipitation kinetics in a super purity Al-0.8 Pct Mg-0.9 Pct Si alloy using differential scanning calorimetry, Metall. Mater. Trans. A 30 (1999) 879–884.
[26] A.D. Le Claire, Solute diffusion in dilute alloys, J. Nucl. Mater. 69&70 (1978) 70–96.
[27] H. Mehrer, Diffusion in Solids, Springer, Berlin, Heidelberg, New York, 2007.
[28] F.D. Fischer, J. Svoboda, F. Appel, E. Kozeschnik, Modeling of excess vacancy annihilation at different types of sinks, Acta Mater. 59 (2011) 3463–3472.
[29] W.M. Lomer, Point defects and diffusion in metals, Institute of Metals, London, 1958.
[30] M.F. Francis, W.A. Curtin, Microalloying for the controllable delay of precipitate formation in metal alloys, Acta Mater. 106 (2016) 117–128.
[31] M. Mantina, Y. Wang, L.Q. Chen, Z.K. Liu, C. Wolverton, First principles impurity diffusion coefficients, Acta Mater. 57 (2009) 4102–4108.
[32] Z. Yang, Multi-stage ageing in an Al-Mg-Si alloy, PhD thesis, Technische Universität Berlin, Berlin, 2019.
[33] M.J. Starink, L.F. Cao, P.A. Rometsch, A model for the thermodynamics of and strengthening due to co-clusters in Al-Mg-Si-based alloys, Acta Mater. 60 (2012) 4194–4207.
[34] J. Friis, S. Gouttebroze, Ø. Nygård, I. Ringdalen, Modelling of clustering in 6xxx aluminium alloys, International Conference on Aluminium Alloys ICAA, Oral presentation, 2020.
[35] S. Esmaeili, D.J. Lloyd, W.J. Poole, Modeling of precipitation hardening for the naturally aged Al-Mg-Si-Cu alloy AA6111, Acta Mater. 51 (2003) 3467–3481.
[36] S. Esmaeili, D.J. Lloyd, W.J. Poole, A yield strength model for the Al-Mg-Si-Cu alloy AA6111, Acta Mater. 51 (2003) 2243–2257.
[37] M.J. Starink, Analysis of aluminium based alloys by calorimetry: quantitative analysis of reactions and reaction kinetics, Int. Mater. Rev. 49 (2004) 191–226.
[38] T. Saito, E.A. Mortsell, S. Wenner, C.D. Marioara, S.J. Andersen, J. Friis, K. Matsuda, R. Holmestad, Atomic structures of precipitates in Al-Mg-Si alloys with small additions of other elements, Adv. Eng. Mater. 20 (2018).
[39] J. Peng, S. Bahl, A. Shyam, J.A. Haynes, D.W. Shin, Solute-vacancy clustering in aluminum, Acta Mater. 196 (2020) 747–758.
[40] M. Mizuno, K. Sugita, H. Araki, Structure and stability of vacancy–solute complexes in Al–Mg–Si alloys, Materialia 13 (2020) 100853.
[41] R. Kobayashi, D. Giofre, T. Junge, M. Ceriotti, W.A. Curtin, Neural network potential for Al-Mg-Si alloys, Phys. Rev. Mater. 1 (2017) 053604.
[42] P. Lang, E. Povoden-Karadeniz, W. Mayer, A. Falahati, E. Kozeschnik, The bustling nature of vacancies in alloys, in: F. Marquis (Ed.) 8th Pacific Rim International Conference on Advanced Materials and Processing, TMS, 2013, pp. 3181-3188.
[43] S.Q. Zhu, H.C. Shih, X.Y. Cui, C.Y. Yu, S.P. Ringer, Design of solute clustering during thermomechanical processing of AA6016 Al-Mg-Si alloy, Acta Mater. 203 (2021) 116455.
[44] R. Ivanov, A. Deschamps, F. De Geuser, Clustering kinetics during natural ageing of Al-Cu based alloys with (Mg, Li) additions, Acta Mater. 157 (2018) 186–195.
[45] A. Jain, A. Glensk, D. Marchant, M. Ceriotti, W.A. Curtin, Vacancy prisons and solute clustering in aluminium alloys, International Conference on Aluminium Alloys ICAA, Oral presentation, 2020.
[46] Y. Aruga, M. Kozuka, Y. Takaki, T. Sato, Formation and reversion of clusters during natural aging and subsequent artificial aging in an Al-Mg-Si alloy, Mater. Sci. Eng. A 631 (2015) 86–96.
[47] V. Fallah, B. Langelier, N. Ofori-Opoku, B. Raeisinia, N. Provatas, S. Esmaeili, Cluster evolution mechanisms during ageing in Al-Mg-Si alloys, Acta Mater. 103 (2016) 290–300.
[48] S. Pogatscher, H. Antrekowitsch, P.J. Uggowitzer, Interdependent effect of chemical composition and thermal history on artificial aging of AA6061, Acta Mater. 60 (2012) 5545–5554.
[49] A. Schulze, K. Lücke, The influence of vacancies on short-range order formation in Au-Ag alloys, Acta Metall. 20 (1972) 529–542.
[50] J.D. Robson, Deformation enhanced diffusion in aluminium alloys, Metall. Mater. Trans. A 51A (2020) 5401–5413.
[51] W.W. Sun, Y.M. Zhu, R. Marceau, L.G. Wang, Q. Zhang, X. Gao, C. Hutchinson, Precipitation strengthening of aluminum alloys by room-temperature cyclic plasticity, Science 363 (2019) 972–975.
[52] J. Røyset, T. Stene, J.A. Sæter, O. Reiso, The effect of intermediate storage temperature and time on the age hardening response of Al-Mg-Si alloys, Mater. Sci. Forum 519-521 (2006) 239–244.